Reactions $He^4(p,tp)p$ and $He^4(p,He^3p)n$ at $E_p = 47$ MeV

J. G. Rogers,* G. Paić,† J. Reginald Richardson, and J. W. Verba
University of California, Los Angeles, California 90024‡
(Received 17 April 1970)

The three-body breakup reactions induced by 47-MeV protons on a gaseous He^4 target have been investigated in a kinematically complete experiment. Protons were observed in coincidence with tritons or He^3's at several pairs of coplanar lab angles using two counter telescopes. Data were stored by an on-line computer which serially listed four linear signals from each event on magnetic tape. The proton spectra showed strong enhancements from neutron-proton and proton-proton final-state interactions, in agreement with the predictions of the Watson-Migdal theory. A Chew-Low–type extrapolation procedure was used to extract the *np* singlet scattering length, which was in fair agreement with the value from *np* free scattering. The triton and He^3 spectra showed peaks due to sequential reaction processes via the continuum resonance states in the He^4 system. These enhancements could be identified with previously observed He^4 levels of known spin and parity assignments.

INTRODUCTION

Any reaction involving three particles in the final state may exhibit distinctive peaks in the energy spectra of emitted particles because of one or more processes. The detailed shapes of spectra are often complex and can be affected by complicated interferences between first-, second-, and higher-order processes as well as possible many-body forces. Because of the complexity of a detailed theoretical treatment of such a problem, data are measured and analyzed in restricted portions of phase space, and the possible occurrence of second-order effects, interference, and many-body forces is neglected. Three basic processes are considered.

The *sequential breakup* is the case in which two of the emerging particles interact strongly with each other in the final state compared to their interactions with the third particle. This classification includes both nucleon-nucleon final-state interactions (FSI) and sequential decay through particle-unstable nuclear levels. Both of these kinds of sequential processes are characterized by a definite relative energy for the pair of particles that "stick together" in the final state, and both may be viewed as two-step processes, sequential in time.

The *simultaneous breakup* is a direct reaction in which the three particles emerge simultaneously in the final state. In the absence of resonant processes and when the scattering matrix is not a function of the way in which the energy is distributed among the emerging particles, this process results in a phase-space distribution. Qualitatively, one might expect a phase-space distribution in the energy spectrum at fixed lab angles when the three emerging particles interact weakly in the final state. It is important to note that the presence of this process is generally assumed but has never been fully proven.

The third process, quasifree scattering, is a direct reaction in which the projectile interacts with a single constituent of the target. In the final state we find the projectile and the scattered constituent with high relative energies and the remainder of the target is left with a low energy in the lab frame.

It is known from other breakup studies[1] that all three of these processes contribute substantially to the spectra of particles emitted in $p+D$ and $p+He^3$ breakup. Since He^4 breakup reactions are not expected to contain significant quasifree contributions at these energies because of the very large Q values involved, they offer an opportunity to study nucleon-nucleon FSI's free from this competing process, an advantage not present in reactions involving the more loosely bound deuteron or He^3 particles. However the spectra, in the case of a He^4 target, reflect not only the nucleon-nucleon final-state interaction but also the nucleon-trion (where trion is a triton or He^3 particle) interaction in the particle-unstable excited states of He^4. The nucleon-nucleon interaction has been studied in a kinematically incomplete measurement of these same reactions,[2] but not with a view toward investigating the dependence of the cross section of nucleon-nucleon low-energy scattering parameters. In the present kinematically complete experiment we have studied the He^4 breakup both from the point of view of nucleon-nucleon interactions and of He^4 excited states.

EXPERIMENTAL METHOD

Single-counter measurements of $He^4(p,t)2p$ and $He^4(p,He^3)pn$ showed that the cross section for the production of the strongly interacting nucleon-nu-

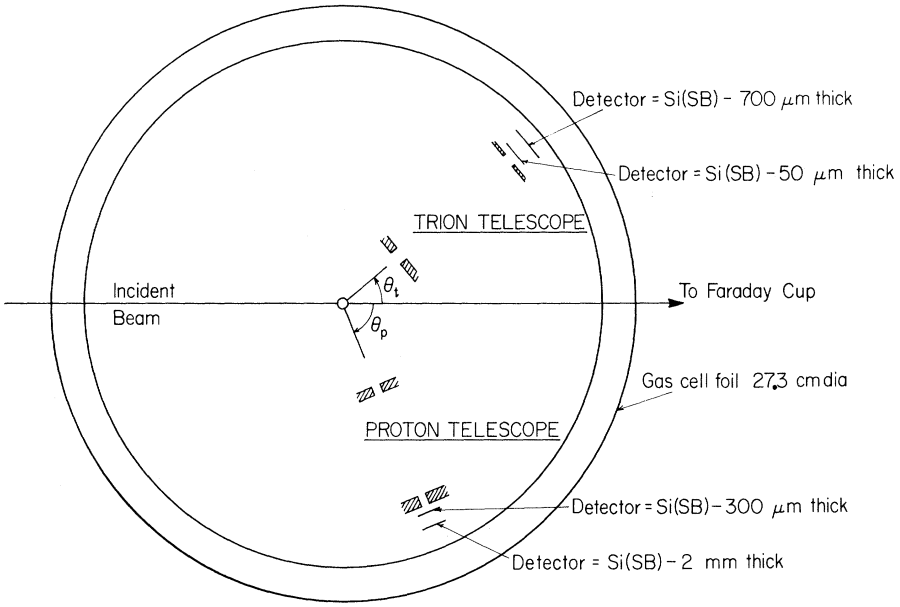

FIG. 1. A scale drawing of the inside of the gas target cell showing the arrangement of the two detector telescopes and the thicknesses of the detectors. The entire region inside the foil contained helium gas. Si(SB) means silicon surface-barrier detector.

cleon pairs in the final state exhibited maxima at very forward angles for trion emission and at about 32° in the lab.[2] The low energy of the protons corresponding to trions emitted at forward angles makes the present measurement in the region of the first maximum impractical. Accidental coincidences and pulse pile up in the electronics were also experimental difficulties encountered when small-angle trion observations were attempted, since the competing two-body reactions are strongly forward peaked.[2,3] We chose to investigate the nucleon-nucleon FSI by measuring the correlated energy spectra at a trion angle of $\theta_t = 40°$ and at three different proton angles, $\theta_p = 51$, 67.5, and 80°. All measurements in the kinematically complete experiment were made with the proton and trion detector telescopes on opposite sides of the beam line, which means that the azimuthal angle between the trion and proton momenta was always $\phi_{tp} = 180°$.

The momentum-analyzed proton beam of the UCLA sector focused cyclotron was used to bombard a natural helium gas target in a cylindrical cell of 27.3-cm outside diameter. The pressure in the cell was kept at about 1 atm. The beam entered through a 50-μ-thick Kapton H–foil window which extended over 330° of the cylinder's circumference. Additional details on the experimental area, shielding, Faraday cup, and gas target cell have been reported previously.[4]

The counter arrangement which was used for acquisition of most of the data is shown in Fig. 1. It consisted of two particle telescopes, each of which contained two silicon surface-barrier detectors operated at room temperature in the helium gas. The thicknesses of the four detectors are also shown in Fig. 1. The detectors were mounted inside the target cell to minimize the energy losses of the scattered particles. We could observe protons down to an energy of 2 MeV, and tritons could be separated from He^3's down to an energy of about 4 MeV. The absolute angular accuracy is estimated at ±0.5°. The two telescopes were always kept in the horizontal plane.

The region of target gas viewed by each detector was defined by a pair of brass slits in each telescope. In such a geometry each telescope views a region of target composed of a central umbra (the region in which the entire rear aperture is exposed) and a wider penumbra (the region in which the rear aperture is partly obscured by the front slit). The intersection of the umbra and penumbra of one telescope with the umbra and penumbra of the other telescope defines the target region effective in a coincidence measurement. The target thickness and the angular acceptances of each telescope are functions of both scattering angles and the sizes and separations of the apertures in both telescopes.[5] The proton and trion telescopes had front apertures of horizontal opening 0.452 and 0.635 cm, respectively, and rear apertures of horizontal opening 0.452 and 0.508 cm. The apertures were 6.17 cm apart in the proton telescope and

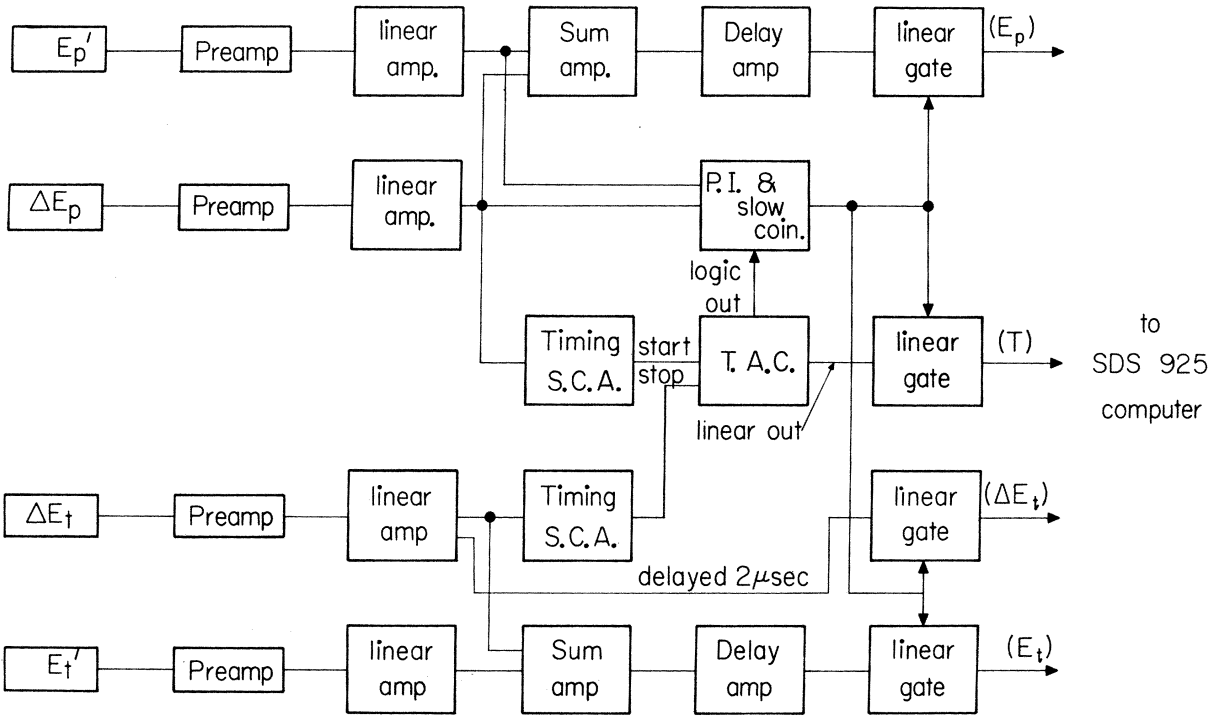

FIG. 2. A simplified schematic block diagram of the electronics used to collect most of the data. The detailed functions of the various elements are described in the text. S.C.A. = single-channel analyzer and T.A.C. = time-to-amplitude converter.

7.15 cm apart in the trion telescope.

For some of the measurements, when it was not necessary to observe the very low-energy protons, the experimental arrangement differed from that described above. For these measurements at θ_t, $\theta_p = 40°$, 51°; 40°, 67.5°; and 30°, 40° the proton telescope was mounted on an independent arm outside the target cell. This telescope consisted of a 250-μ-thick plastic scintillator optically coupled to a Phillips 56AVP photomultiplier tube as a ΔE detector, and a NaI(Tl) crystal optically coupled to a RCA 8053 photomultiplier as an E detector. This arrangement set a lower limit of about 5 MeV for the observation of protons.

Each coincidence event generated four linear signals; the energy loss (ΔE_p) of particles in the proton telescope passing counter, the residual energy (E_p') deposited in the proton telescope stopping counter, the energy loss (ΔE_t) of particles in the trion passing counter, and the residual energy (E_t') deposited in the trion stopping counter. A block diagram of the circuit used in the setup with the detectors inside the gas cell is presented in Fig. 2. Two timing signals from the E detectors triggered a time-to-amplitude converter, the output of which (T) was stored as a measurement of the relative arrival time of the two particles observed. The other linear signals that were stored by the on-line computer were the linear sum of E' and ΔE from each telescope, which are labeled $E_p(=\Delta E_p + E_p')$ for the proton and $E_t(=\Delta E_t + E_t')$ for the trion in Fig. 2, and the energy loss of the trions in the passing counter, labeled ΔE_t in Fig. 2.

The final important element of the electronic arrangement is the element labeled "P.I. and slow coincidence" in the block diagram. This auxiliary circuit included a Goulding-type particle identifier which was used to reject all deuterons observed in the proton telescope. The largest rate of such particles was from the $He^4(p,d)He^3$ reaction, since at some of the pairs of angles examined, the deuteron entered the proton telescope and the recoil He^3 entered the trion telescope. With perfect experimental resolution these two-body events would be separated kinematically from the locus of the three-body events; however, the finite energy and angular resolution of the detection system caused the two types of events to overlap sufficiently at some angles to make the particle-identifier circuit necessary. In addition to the requirement that the particle observed in the proton telescope not be a deuteron, an over-all slow (1 μsec) coincidence was required between the four signals to be stored by the computer.

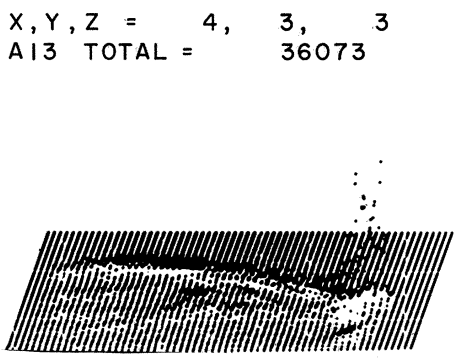

FIG. 3. A photograph of the isometric oscilloscope projection of the raw data in an E_t versus E_p array for $\theta_t = 40°$, $\theta_p = 51°$. The ellipse-shaped contour across the upper part of the display is formed by the overlapping three-body loci of the reactions $He^4(p,tp)p$ and $He^4(p, He^3p)n$.

The linear signals were converted by four analog-to-digital converters with 1024-channel resolution. The computer listed these pieces of information on magnetic tape in serial order and also formed a two-dimensional 64×64 array of counts from a selected pair of signals which could be viewed continuously as an isometric oscilloscope display. Figure 3 shows a picture of a typical E_t versus E_p array from the oscilloscope.

The electronics setup described thus far applies to data acquisition using the four surface-barrier detectors inside the gas cell and was modified somewhat to process the four signals when the plastic scintillator and NaI crystal were used. With the latter counter arrangement, the Goulding particle identifier was not employed, since this arrangement was used only at angles where the two-body events were kinematically well separated from the events of interest. The ΔE_p scintillator supplied only a timing pickoff; the linear signal information from this detector was not used.

DATA AND ANALYSIS

The three-body loci at the sets of angles examined for the nucleon-nucleon FSI are shown for the $He^4(p, He^3p)n$ reaction in Fig. 4, where the solid curve is the He^3 energy (E_H) versus E_p locus, and the dash-dot curve is the np relative energy (E_{np}) versus E_p. As one sweeps the proton counter from $\theta_p = 51$ to 67.5° the minimum relative energy of the two nucleons varies from $E_{np}(\min) = 0.8$ MeV to $E_{np}(\min) = 0$. As the proton angle is further increased, the minimum relative energy rises again to 0.5 MeV at 80°. The kinematic loci for the $He^4(p, He^3p)n$ reaction are very similar to those for $He^4(p,tp)p$, as can be seen from Fig. 5, where the corresponding set of kinematic loci for the latter reaction are shown.

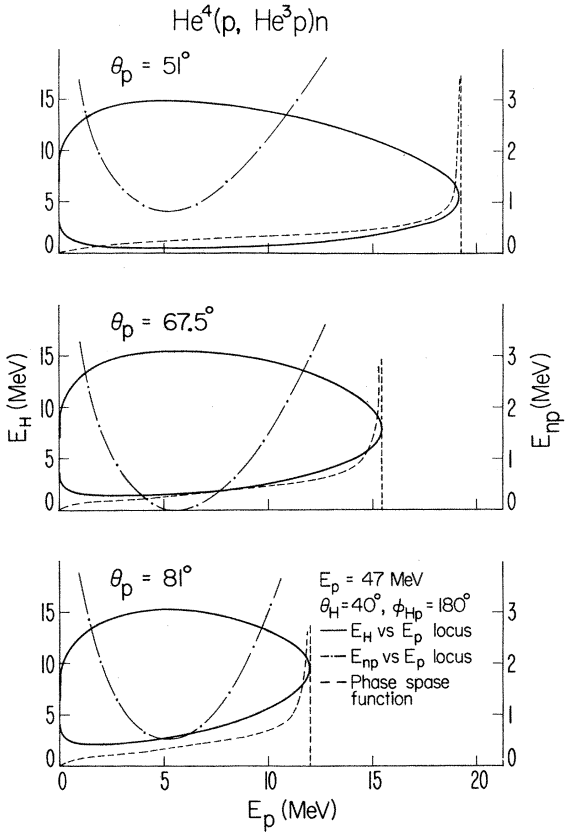

FIG. 4. $He^4(p, He^3p)n$ three-body kinematic loci for three sets of measured angles as predicted by a relativistic kinematic calculation. The solid curve, the He^3 energy E_H versus E_p locus, is appropriate for comparison with the two-dimensional array, as shown in Fig. 3. The dash-dot curve, the locus of relative energy E_{np} versus E_p, is relevant to events falling on the upper branch of the E_H versus E_p locus, and is useful in identifying peaks due to the expected $^1S_0$ FSI in the np system. The phase-space function along the upper branch (dashed curve) is slowly varying in the region of minimum np relative energy but is peaked at the high-energy end of the proton spectrum.

The third (dashed) curve plotted in Figs. 4 and 5 is proportional to the volume of phase space available for the reaction products as a function of proton energy. Both the relative-energy locus and the phase-space function refer to the upper branch of the double-valued E_t versus E_p function. Projection of data on the proton energy axis is appropriate for investigating the nucleon-nucleon FSI, since the phase space is smooth in the region of low nucleon-nucleon relative energies in the proton spectrum. This is in contrast to a spectrum projected on the trion axis, which would be expected to show a phase-space peak in the region of minimum nucleon-nucleon relative energies even in

the absence of any sequential process. Such a phase-space peaking is exactly calculable, but the effects of finite angular and energy resolution on such a fast-rising cross section make the extraction of information from superimposed features very uncertain.

The data recorded on magnetic tape by the acquisition program were reduced by a separate off-line computer program to projected spectra of counts versus channel number for the two reactions of interest. The basic technique was to read the data tape into the computer to form various one- and two-dimensional arrays of counts versus channel number for selected events from the tape. This procedure is illustrated for a particular data set in Figs. 3, 6, and 7, which are photographs of an oscilloscope display during various steps of the data reduction.

Figure 3 is the unfiltered 64×64 channel E_t versus E_p array of all the reaction events observed in the $p + He^4$ breakup. Figure 6(a) shows the unfiltered ΔE_t versus E_t telescope array formed from the same data. Figure 6(b) shows "filter function" lines which were calculated by the program to isolate the He^3 particles from all the others in the telescope array. Figure 6(c) is a 512-channel time spectrum formed from the data with the filter requirement of Fig. 6(b). The events in the large central peak are the true coincidence events. Figure 7(a) is of the data extracted from that shown in Fig.

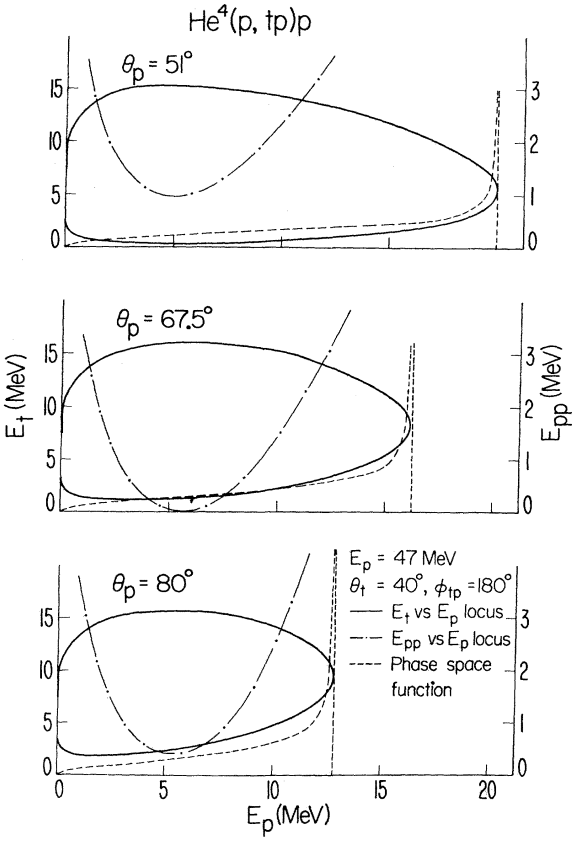

FIG. 5. $He^4(p,tp)p$ three-body kinematic loci for three sets of measured angles. For further details see the caption for Fig. 4.

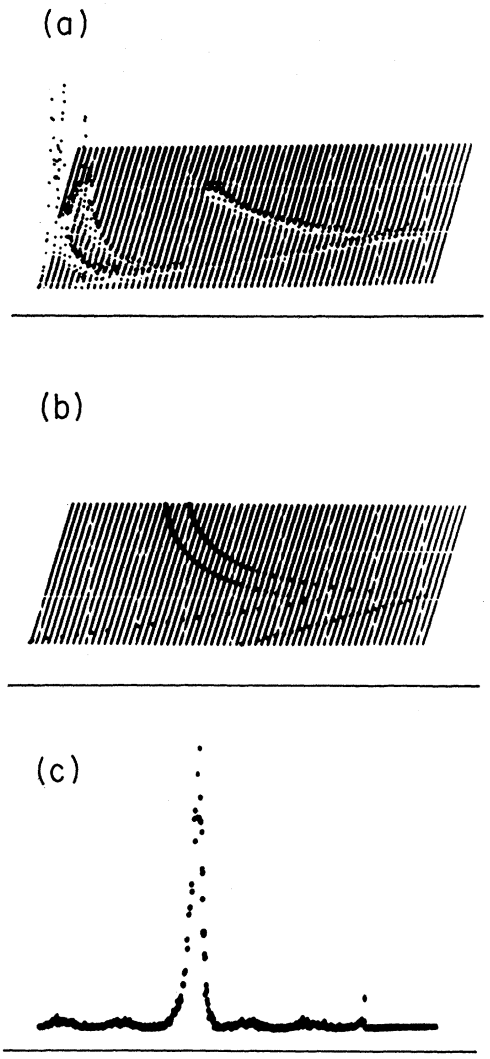

FIG. 6. (a) A telescope array (ΔE_t versus E_t) showing the $Z = 1$ particles to the left and the He^3 particles in the center and to the right. The diagonal straight-line portion is caused by He^3 particles which stop in the passing counter of the trion telescope. (b) Particle division contours intensified in the ΔE_t versus E_t array, with the data suppressed from the display. These contours separate the He^3 particles from all other particle types observed in the trion telescope for all trion energies above about 4 MeV. (c) A time spectrum for the He^3 particles selected by the contours in (b). This spectrum shows the large peak of true coincidence events and smaller peaks of random events, which are separated from each other by intervals equal to the cyclotron rf period (35 nsec.).

3 by applying the filter of Fig. 6(b) and the requirement that the time coordinate of the events be located within the peak for the true coincidence events on Fig. 6(c). Figure 7(b) and Fig. 7(c) are the final projections of the counts of Fig. 7(a) on the vertical and horizontal energy axes with an additional filter requirement set to exclude the events which do not lie on the kinematic locus for the $He^4(p,He^3p)n$ reaction. To make a reasonable compromise between statistics and channel resolution,

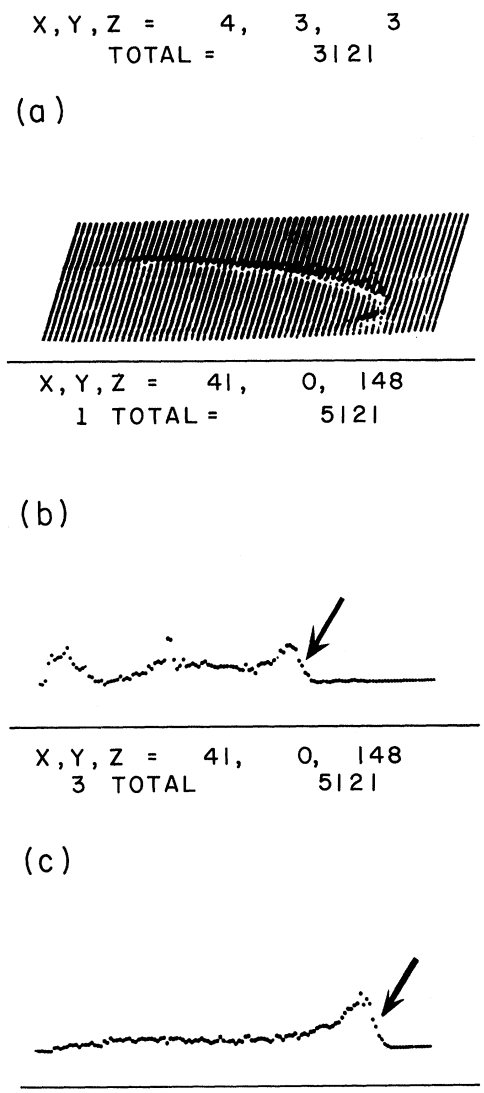

FIG. 7. (a) The kinematic locus for $He^4(p,He^3p)n$ true coincidence events, which was separated from the raw data shown in Fig. 3 using the methods described in the text. (b) The locus of (a) projected on the vertical trion axis excluding all events off the proper three-body locus. The sharp peak (two channels) in the center is an instrumental effect. (c) The locus of (a) projected in the horizontal E_p axis, excluding the events off the locus.

this last projection was performed using 128 channels. The projected spectra of counts were transformed to units of mb/sr^2 MeV using the measured integrated beam current, target density, and detector geometries. Details of this calculation will be the subject of a later article.[6]

We found that simple sequential theory[7] gave a rather good prediction of the enhancement in the proton spectra due to the nucleon-nucleon FSI. The theoretical prediction was calculated as a function of proton lab energy and a Gaussian resolution function was folded in. The width of this Gaussian resolution function was determined by applying the same folding to the phase-space functions shown in Figs. 4 and 5 so that they matched the slope of the observed projected spectra along the falling edge of the high-energy kinematic end points, the regions indicated by arrows in Fig. 7(b) and Fig. 7(c). Since the unbroadened phase-space functions are vertical in this region, the finite *slope* of the experimental data is a measure of the combined angular and energy resolution of the detector system. The *position* of the high-energy cutoff was adjusted to match the phase-space function by varying the energy calibration constants, i.e., the gain and offset. The average result of this determination for the several proton spectra was a width of 1.0 MeV full width at half maximum (FWHM) for the Gaussian resolution function. We attribute the larger part of this 1.0 MeV to kinematic broadening due to the angular acceptance of the counters.

The differential cross section at $\theta_t = 40°$, $\theta_p = 67.5°$ is shown in Fig. 8 for the $He^4(p,tp)p$ reaction. The double peaking on either side of $E_p = 5.5$ MeV is due to the *pp* FSI. The Watson-Migdal (WM) theory gives a fairly good prediction of the shape of the *pp* peaks, as shown by the solid curve in Fig. 8.

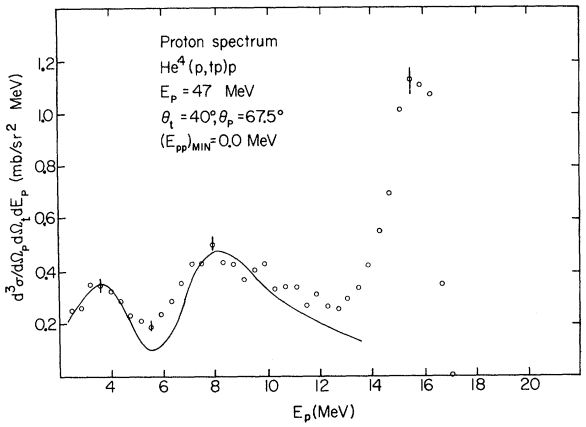

FIG. 8. The proton spectrum from $He^4(p,tp)p$ at $\theta_t = 40°$, $\theta_p = 67.5°$ in mb/sr^2 MeV. The solid curve is the prediction of the Watson-Migdal theory. Typical error bars due to statistics are also shown.

In the absence of the Coulomb force the WM theoretical expression predicts a single peak centered at $E_{pp}=0$. The width of this peak is related directly to the size of the scattering length, a smaller width for a larger absolute value of the scattering length. The effect of the Coulomb interaction is to depress the cross section at the very lowest relative energies, since the Coulomb force in the theory is infinitely repulsive at $E_{pp}=0$ and entirely swamps the attractive nuclear force. This depression causes the minimum at $E_p=5.5$ MeV. Since the the Coulomb penetration factor $C(\eta)$ falls off exponentially with decreasing pp relative energy,[8] the Coulomb effect is most significant in the vicinity of $E_{pp}=0$. This spectrum shape, which characterizes the pp FSI, has been seen previously in $p+D$, $p+\mathrm{He}^3$, and $\mathrm{He}^3+\mathrm{He}^3$ reactions.[9]

If a proton angle is chosen to exclude the pp relative energies below 0.4 MeV [$E_{pp}(\mathrm{min})=0.4$ MeV] from observation, it is expected that a single broad peak will be observed for the pp FSI. This was found to be the case at $\theta_p=80°$, as shown in the spectrum of Fig. 9. The pp FSI peak is still in fair agreement with the WM theory (solid line) at this set of angles. Figure 10 shows the spectrum at $\theta_p=51°$, where $E_{pp}(\mathrm{min})=1.0$ MeV. At these high relative energies the assumptions of the WM theory are violated, and the cross section in the vicinity of the minimum pp relative energy ($E_p=5.5$ MeV) can no longer be expected to be dominated exclusively by an S-state nucleon-nucleon FSI process.

In these three spectra, and the ones to follow for the $\mathrm{He}^4(p,\mathrm{He}^3p)n$ reaction, the solid curves represent the WM theoretical prediction with the values of the low-energy nucleon-nucleon scattering parameters determined from nucleon-nucleon scattering.[8] The curves are independently normalized to fit the FSI peak at each angle. The peak near the high-energy proton end point is probably due mainly to phase-space peaking. However, this peak may also be augmented by enhancements due to the sequential processes via the particle-unstable levels in the $A=4$ system.

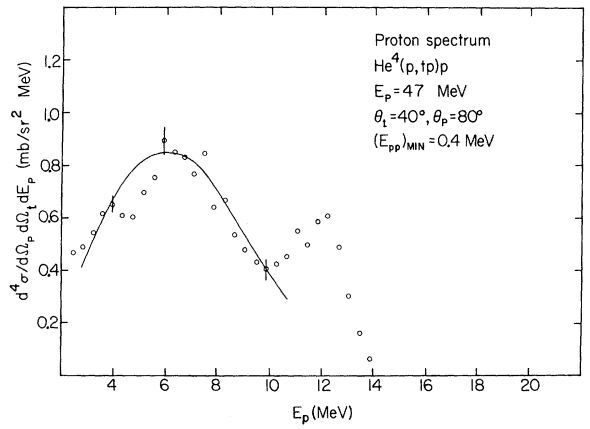

FIG. 9. The proton spectrum from $\mathrm{He}^4(p,tp)p$ at $\theta_t=40°$, $\theta_p=80°$ in mb/sr^2 MeV. See the caption for Fig. 8.

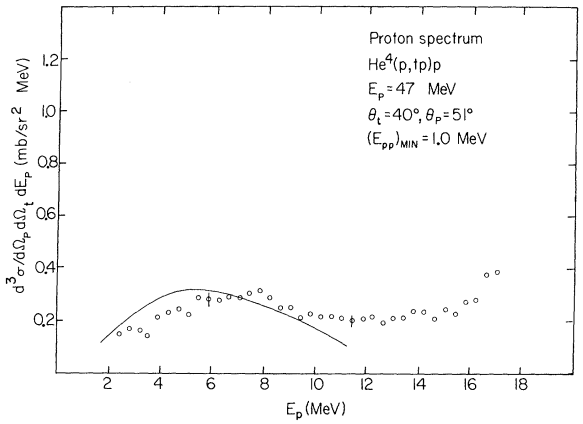

FIG. 10. The proton spectrum from $\mathrm{He}^4(p,tp)p$ at $\theta_t=40°$, $\theta_p=51°$ in mb/sr^2 MeV. See the caption for Fig. 8.

The proton spectrum for the reaction $\mathrm{He}^4(p,\mathrm{He}^3p)n$ at $\theta_H=40°$, $\theta_p=67.5°$ is shown in Fig. 11. Because of the great similarity of the kinematics, all relative energies from zero upward are kinematically allowed in the np system at this set of angles, which is appropriate to $E_{pp}(\mathrm{min})=0$ in the $\mathrm{He}^4(p,tp)p$ reaction. As expected, in the absence of Coulomb forces, the spectrum exhibits a single strong peak in the region of low np relative energies. The np singlet scattering length is appreciably larger in absolute value than the corresponding pp scattering length, so the np FSI peak is considerably narrower than the (split) pp FSI peak. The width of this peak is about 160 keV (FWHM) in

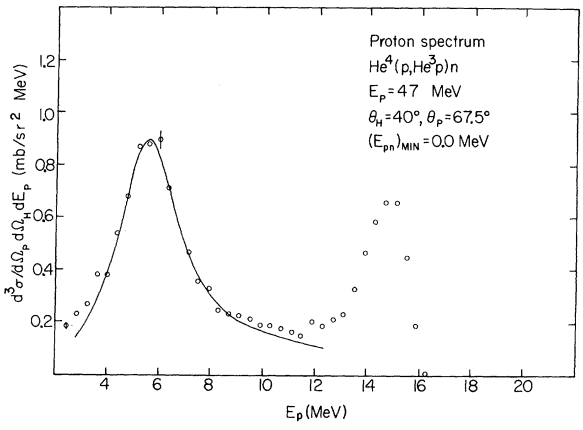

FIG. 11. The proton spectrum from $\mathrm{He}^4(p,\mathrm{He}^3p)n$ at $\theta_H=40°$, $\theta_p=67.5$ in mb/sr^2 MeV. See the caption for Fig. 8.

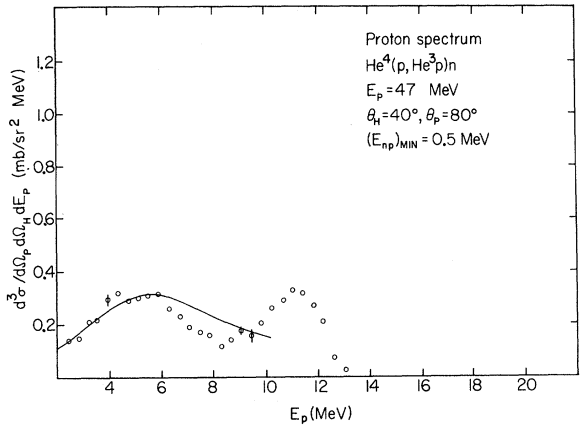

FIG. 12. The proton spectrum from $He^4(p, He^3p)n$ at $\theta_H = 40°$, $\theta_p = 80°$ in mb/sr^2 MeV. See the caption for Fig. 8.

np relative energy, whereas the *pp* peak is about 1.6 MeV wide.

The effect of the *np* triplet interaction is difficult to account for in a meaningful way using the WM theory. In a somewhat unsophisticated treatment, one can add an incoherent triplet mixture weighted only by the relative statistical factor of that final state. The solid curve shown in Fig. 11 represents an incoherent sum of triplet and singlet S-state *np* interactions as predicted by the WM theory. The triplet admixture was weighted by a factor of 3, which is the spin multiplicity of the triplet *np* final state relative to the singlet.[10] The over-all cross section ($\sigma_s + 3\sigma_t$) was broadened by the Gaussian resolution function and normalized at the maximum of the FSI peak of the experimental data to obtain the curve shown. The triplet *np* scattering length is much smaller than the singlet in absolute value, so the relative effect of the additional term on the shape is negligible in the vicinity of $E_{np} = 0$.

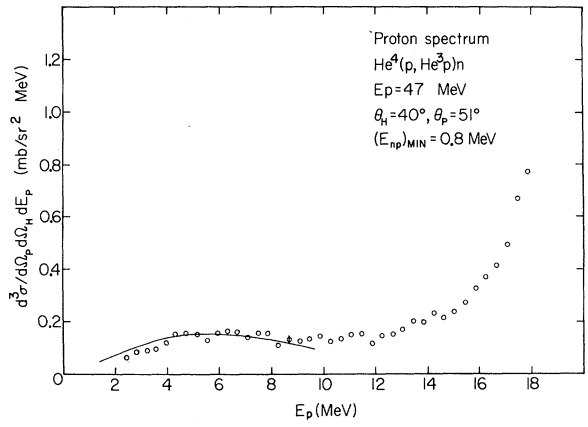

FIG. 13. The proton spectrum from $He^4(p, He^3p)n$ at $\theta_H = 40°$, $\theta_p = 51°$ in mb/sr^2 MeV. See the caption for Fig. 8.

As we sweep the proton angle away from the one where $E_{np}(\min) = 0$, the FSI peak decreases sharply. The differential cross section at $\theta_p = 80°$ is shown in Fig. 12. The contribution of the $^3S_1$ *np* reaction relative to the $^1S_0$ is expected to be greater at these higher relative energies. At $\theta_p = 51°$ the spectrum shown in Fig. 13 does not exhibit any particular peak in the region of $E_{np}(\min) = 0.8$ MeV. It is likely that the influence of the *np* FSI on the spectrum at these relative energies is predominantly due to a $^3S_1$ interaction. It is also likely that an adequate description of the final state under these circumstances must include the effect of the presence of the He^3 particle. This is especially necessary in view of the possibility of resonant He^3-*n* in-

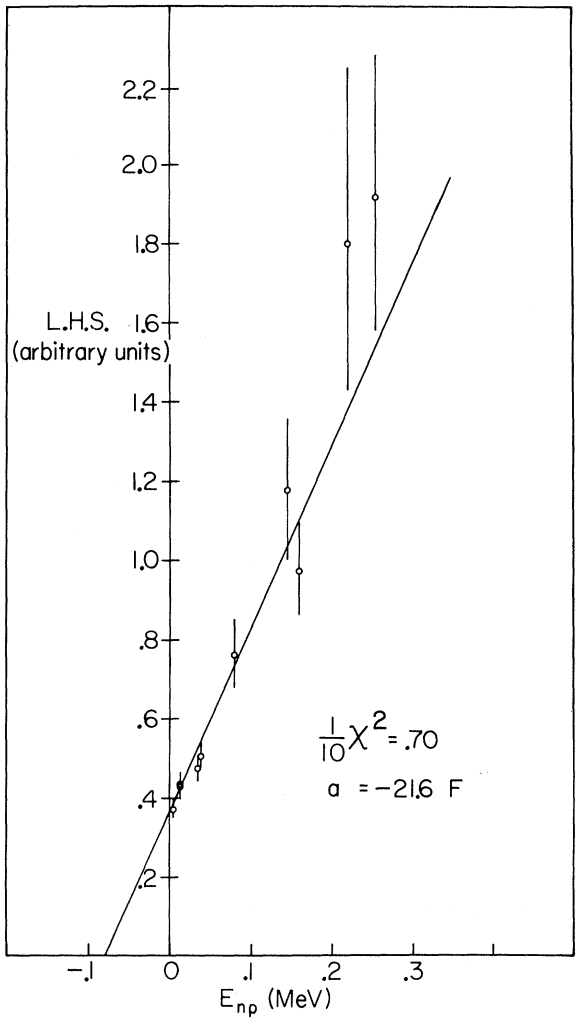

FIG. 14. A plot of the function on the left-hand side of Eq. (2) versus the *np* relative energy E_{np} for the data from $He^4(p, He^3p)n$ at $\theta_H = 40°$, $\theta_p = 67.5°$. Also shown is the line giving the best χ^2 fit to the 10 data points. The line intercepts the E_{np} axis at $E_{np} = 0.0795$ MeV, which gives the *np* singlet scattering length $a_s = -21.6$ F.

teractions via the levels in He^4 at relative energies of about 8 MeV in the He^3-n system,[11] which also occur in the region near $E_p = 5$ MeV.[2]

Although the WM theory gave a good fit to the experimental data using the currently accepted values of the low-energy np scattering parameters, it is of interest to determine what value of the scattering parameters best fitted the data. To do this we used a linear extrapolation procedure similar to that used by Brückman, Kluge, and Schänzler.[12] To begin with, we wrote the differential cross section as a sum of two terms, one for singlet and one for triplet.

$$\sigma = \sigma_s + \sigma_t ,$$

$$\sigma = \rho \left(\frac{G_1}{k^2 + (-1/a_s + \frac{1}{2} r_{0s} k^2)^2} + \frac{G_2}{k^2 + (-1/a_t + \frac{1}{2} r_{0t} k^2)^2} \right) , \tag{1}$$

therefore

$$\left[\frac{\sigma}{G_2 \rho} - (k^2 + a_t^{-2})^{-1} \right]^{-1} = \frac{1}{G_1 G_2} \left[\left(1 - \frac{r_{0s}}{a_s} \right) k^2 + a_s^{-2} \right] . \tag{2}$$

We have ignored $\frac{1}{2} r_{0t} k^2$ relative to $1/a_t$ and $\frac{1}{4} r_{0s}^2 k^4$ relative to $1/a_s^2$ since we intend to use only data for low values of E_{np}. The subscripts s and t refer to the appropriate $^1S_0$ or $^3S_1$ scattering parameters, respectively, and ρ is the invariant three-body phase-space function.[13] If we plot the expression on the left-hand side of Eq. (2) versus E_{np} ($= \hbar^2 k^2 / 2m$) using the experimental cross section, we should find the points described by a linear function which crosses the E_{np} axis at a point which uniquely determines the singlet np scattering length a_s, since at this crossing point the bracketed term in the right-hand side of Eq. (2) is zero. That is

$$(1 - r_{0s}/a_s) k^2 + a_s^{-2} = 0 , \tag{3}$$

therefore

$$a_s = \tfrac{1}{2} r_{0s} - (\tfrac{1}{4} r_{0s}^2 - \hbar^2 / 2m E_{np})^{1/2} , \tag{4}$$

where m is the reduced mass of the np system, and $\hbar^2 / 2m E_{np} = k^{-2}$. We have assumed the singlet scattering length to be negative in selecting the negative root of the quadratic Eq. (3). This zero crossing is at the value of k where the denominator of the first term in Eq. (1) is zero, the position of a singlet pole in the S matrix.[14] The factor G_2 was determined by normalizing the second term in Eq. (1) to the experimental data at $E_p = 11.0$ MeV. At this point $E_{np} = 2.13$ MeV, and the $^3S_1$ np interaction was assumed to dominate the cross section. The extrapolation of this function for the data from He^4-$(p, He^3 p)n$ at $\theta_H = 40°$, $\theta_p = 67.5°$, is shown in Fig. 14. The line shown in this figure is the one giving the minimum χ^2 for 10 points near $E_{np} = 0$, with the uncertainties taken to be purely statistical, that is,

$$\text{uncertainty} = \frac{df(\sigma)}{d\sigma} \delta\sigma ,$$

where $f(\sigma)$ is the function of the left of Eq. (2), and $\delta\sigma$ is the statistical uncertainty in the cross section. With this procedure we determined the $^1S_0$ np scattering length giving the best fit to the data to be $a_s = -21.6 \pm 2.0$ F. The uncertainty quoted is a sum of the variations in the extracted scattering length due to statistical uncertainty in determining G_2(±1.0 F) and to the uncertainty in the absolute energy calibration for E_p(±1.0 F). It contains, however, no estimate of any theoretical uncertainty involved in this extrapolation procedure. The uncertainties were determined by recalculating the scattering length after shifting the normalization by one standard deviation or the energy calibration by ±0.10 MeV.

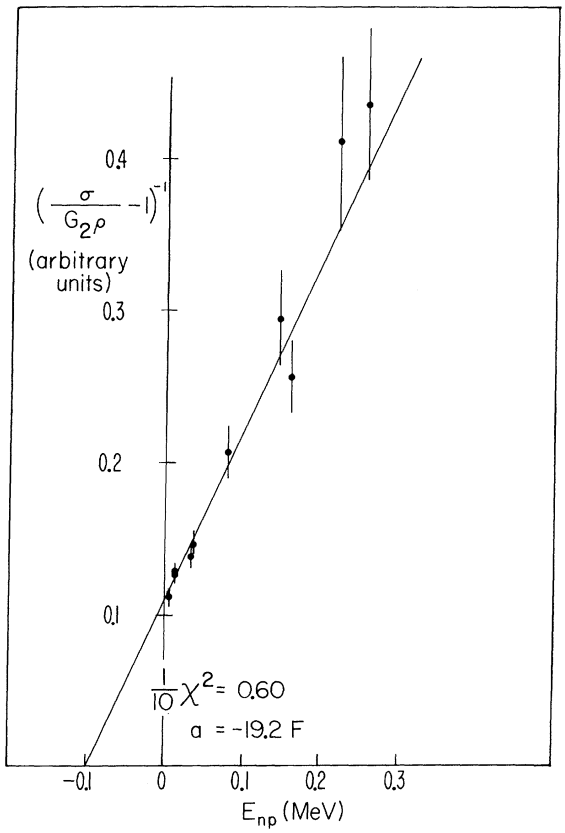

FIG. 15. A plot similar to Fig. 14 but with the triplet term replaced by a pure phase-space term. The straight line giving the best fit intercepts the E_{np} axis at $E_{np} = 0.0991$ MeV, which gives $a_s = -19.2$ F.

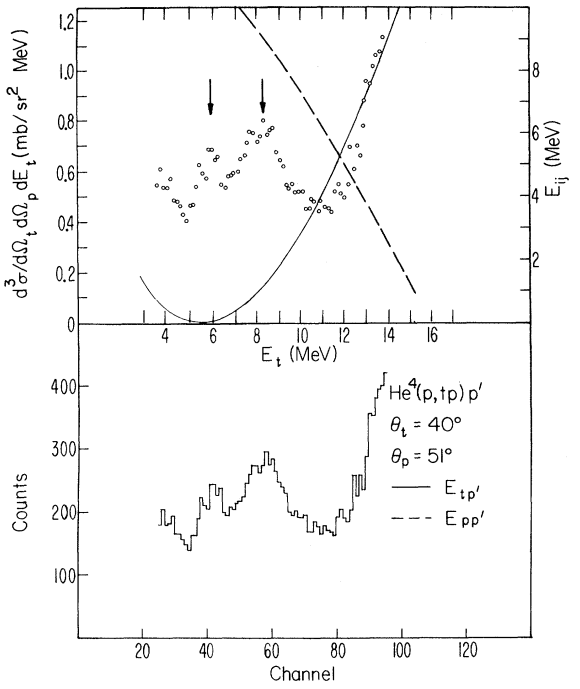

FIG. 16. A triton spectrum as a function of triton energy E_t from the $He^4(p,tp)p$ reaction, showing peaks (indicated by arrows) which are due to He^4 levels. The histogram shows the actual number of counts in each channel, whereas the upper points are these same data converted to differential cross sections (mb/sr^2 MeV). The relative energies are also plotted wherever they are less than 10 MeV.

If the second term in the bracket of Eq. (1) is replaced by a constant term, a similar linear extrapolation may be performed. This extrapolation is shown for the same data in Fig. 15, yielding a scattering length of -19.2 ± 2.0 F for the best fit. As shown in the figures, both of these extrapolations have small values of χ^2 for the line giving the best fit, and both of the extracted scattering lengths are slightly lower in absolute value than the presently accepted $a_s = -23.68$ F from low-energy np scattering data.[14]

It is not possible with such an extrapolation procedure to unfold the effects of finite energy and angular resolution on the value of the scattering length extracted. However, qualitative arguments indicate that insofar as the resolution effects are well represented by Gaussian folding, they tend to cause the value of the extracted scattering length to be too low in absolute value.[15] Thus it seems likely that the departure of the extracted scattering lengths from the "true" scattering length is due in part to experimental resolution effects.

In addition to the peaks discussed in the previous section, enhancements occurred along the three-body kinematic locus in regions where the nucleon-nucleon relative energy is high and the trion-nucleon (either $He^3 - n$ or tp) relative energy is low. These peaks are best examined in a projection of the locus of counts onto the trion axis.

A typical projection onto the triton axis is shown

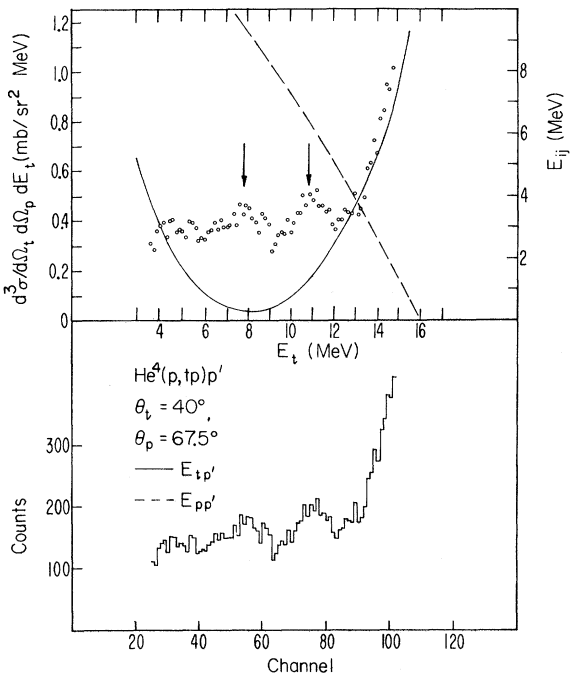

FIG. 17. Triton spectrum: See the caption of Fig. 16.

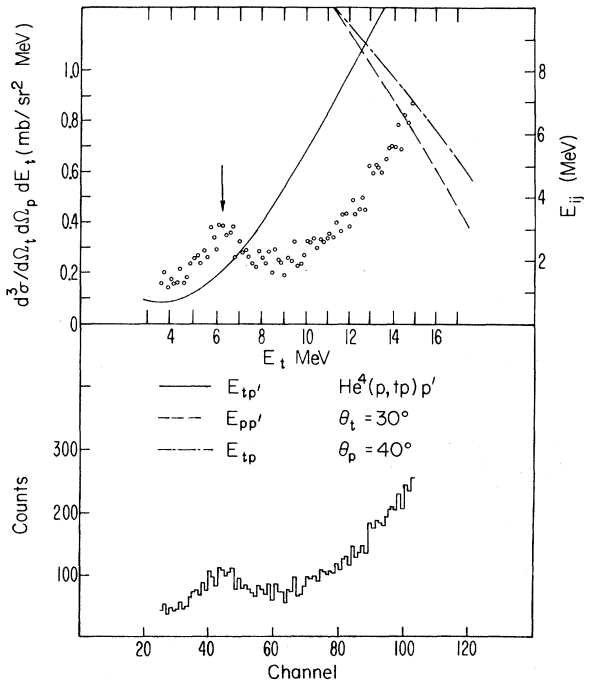

FIG. 18. Triton spectrum: See the caption of Fig. 16.

TABLE I. He^4 levels from $He^4(p,tp)p$. E_{tp} is the relative energy of the observed peak in the triton-proton c.m. system. E^* is that same energy relative to the He^4 ground state. Γ(FWHM) is the approximate width of the peak (measured in relative energy) at the half-maximum of the portion of the peak which is above the background. The last two columns give the characteristics of the nearest He^4 levels as determined from two-body trion-nucleon data. All energies are in MeV.

θ_t θ_p	E_{tp}	E^*	Γ(FWHM)	J^π [a]	E^*_{tb} [a]
40° 51°	0.1 ± 0.1	19.9 ± 0.1	0.15 ± .05	0^+	20.2
	1.1 ± 0.2	20.9 ± 0.2	1.4 ± 0.2	0^- and 2^-	21.4 and 22.4
40° 67.5°	0.3 ± 0.1	20.1 ± 0.1	0.2 ± 0.1	0^+	20.2
	1.4 ± 0.2	21.2 ± 0.2	1.4 ± 0.2	0^- and 2^-	21.4 and 22.4
30° 40°	1.9 ± 0.2	21.7 ± 0.2	1.6 ± 0.3	0^- and 2^-	21.4 and 22.4

[a] J^π and E^*_{tb} are from Ref. 11.

for the $He^4(p,tp)p'$ reaction at $\theta_t = 40°$, $\theta_p = 51°$ in Fig. 16. (The prime is to distinguish the unobserved proton from the observed one.) There are two prominent peaks, one centered at a triton energy of 6 MeV and one at about 8.2 MeV.

To identify the peaks as a function of triton-proton relative energy ($E_{tp'}$), we have plotted that energy as a function of E_t in the same figure. This relative energy is the energy in the c.m. system of the triton and the undetected proton. The other triton-proton relative energy (E_{tp}) is necessarily quite large, since we only observe triton-proton pairs which emerge in approximately opposite directions with enough energy to make detection possible. The pp' relative energy is also high in the region of the peaks, as shown similarly by the plot of that energy in the figure. The energy $E_{tp'}$ is the only one of the three relative energies which is low in the vicinity of the peaks, and sequential enhancements with small energy widths are not expected above 10 MeV in the tp or pp systems. Hence, we may interpret the observed peaks as being due to tp continuum states, which is to say He^4 levels.

The other two prominent features of the data presented are the apparent presence of a large background of nonresonant processes which fills in the regions under the peaks, and the sharp rise above $E_t = 12$ MeV. This rise may be attributed to a combination of phase-space peaking and pp FSI enhancement in this region of low pp relative energy.

Spectra for the $He^4(p,tp)p'$ reaction for three sets of lab angles were analyzed in terms of peak positions in relative tp energy and (wherever possible) corresponding widths. By width, we mean the full width at the half-maximum point of the part of the peak which is above the background. This value is probably lower than the true width, since a part of the "background" is no doubt due to the overlap of the peaks themselves. The triton spectra at θ_t, $\theta_p = 40°$, 67.5°, and 30°, 40° are shown in Figs. 17 and 18. The positions and widths of the observed peaks in the triton spectra are summarized in Table I.

We observe the 0^+ level at excitation energy $E^* = 20.2 \pm 0.2$ MeV and a peak due to a p-wave resonance. The location of this p-wave resonance agrees approximately with the energy of the broad 0^- and 2^- states identified by Meyerhof and Tombrello.[11] The errors quoted here and in Tables I and II are rough estimates of the uncertainties in positions and widths due to statistics, and do not include any possible systematic errors. The variation of the peak position with angle for the p-wave resonance is difficult to analyze in the absence of experimental data at a reasonably complete set of lab scattering angles.

The $He^4(p,He^3p)n$ reaction also shows peaks in the He^3 spectrum which may be identified with levels in He^4. Table II summarizes the analysis of peaks appearing in the three He^3 spectra shown in

TABLE II. He^4 levels from $He^4(p,He^3p)n$. E_{Hn} is the relative energy of the observed peak in the He^3-neutron c.m. system. E^* is that same energy relative to the He^4 ground state. The other columns are described in the heading of Table I. All energies are in MeV.

θ_H θ_p	E_{Hn}	E^*	Γ(FWHM)	J^π [a]	E^*_{tb}
40° 51°	0.8 ± 0.2	21.4 ± 0.2	1.3 ± 0.2	0^- and 2^-	21.4 and 22.4
	$2.6^{+0.2}_{-0.4}$	$23.2^{+0.2}_{-0.4}$	?	?	?
40° 67.5°	1.2 ± 0.2	21.8 ± 0.2	1.2 ± 0.2	0^- and 2^-	21.4 and 22.4
30° 40°	1.5 ± 0.4	21.1 ± 0.4	1.8 ± 0.4	0^- and 2^-	21.4 and 22.4

[a] J^π and E^*_{tb} are from Ref. 11.

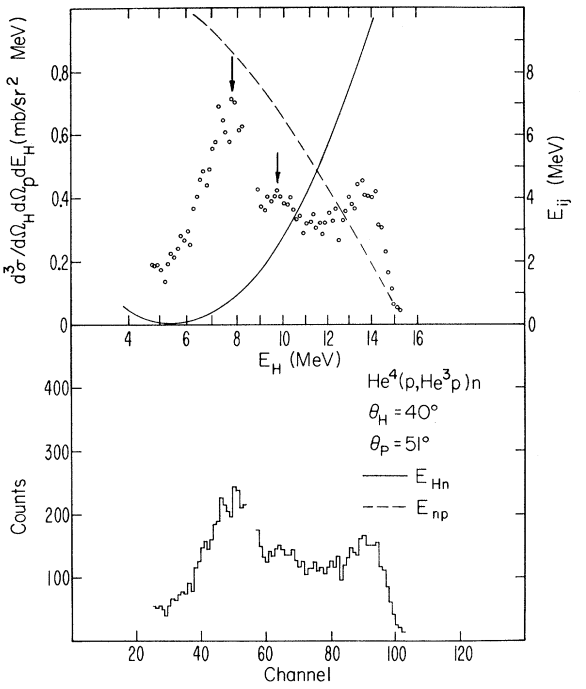

FIG. 19. A He^3 spectrum as a function of He^3 energy E_H from the $He^4(p, He^3p)n$ reaction showing a peak due to the levels of He^4. See the caption of Fig. 16.

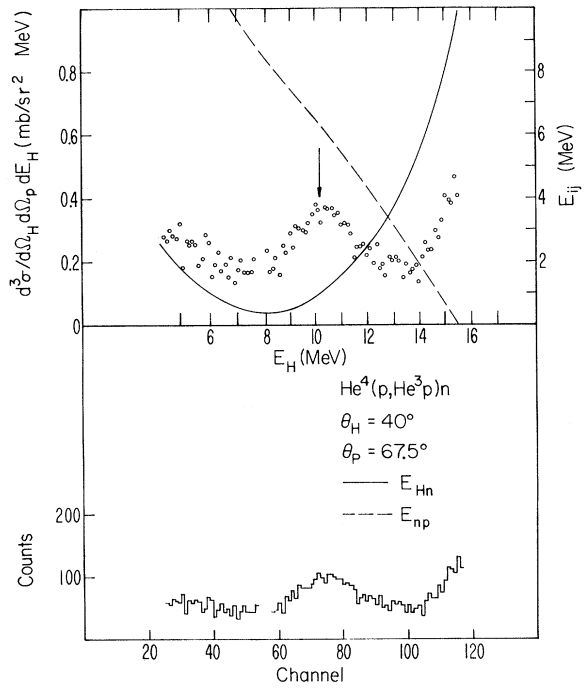

FIG. 20. He^3 spectrum: See the caption for Fig. 19.

Figs. 19, 20, and 21. In the spectra at θ_H, $\theta_p = 40°$, 51° and 40°, 67.5°, the peaks which we attributed to the p-wave resonance are very similar in appearance and width to the corresponding peaks in the triton spectra, but they appear 0.5–0.6 MeV higher in excitation energy. This difference in energy is possibly due to differences in the two reaction channels and perhaps a different penetration factor in the tp channel because of the Coulomb interaction. Alternately, the apparent position of this peak may be affected in the triton channel by its partial overlap with the adjacent 0^+ level, which does not occur in the He^3 channel.

Relative to the background, the He^3 spectra show a stronger yield in the p-wave peak than do the triton spectra. This is in agreement with the corresponding branching ratio found in the kinematically complete study of sequential enhancements in Li^6-$(d,\alpha t)p$ and $Li^6(d,\alpha He^3)n$ at $E_d = 10$ MeV.[16] Except for the p-wave peak, there are no peaks in the He^3 spectra which can be readily identified with the levels of Ref. 11. The He^3 spectrum does however, show a faint indication of a peak at $E^* = 23.2$ MeV (at 40°, 51°), but it is almost statistically insignificant.

Kinematically complete observations have also been reported on the reactions $d + He^3 \rightarrow p + p + t$ or $p + n + He^3$ at $E_{He^3} = 31.8$ MeV[17] and at lower deuteron bombarding energies.[18] The trion spectra from these reactions also showed the peaks correspond-

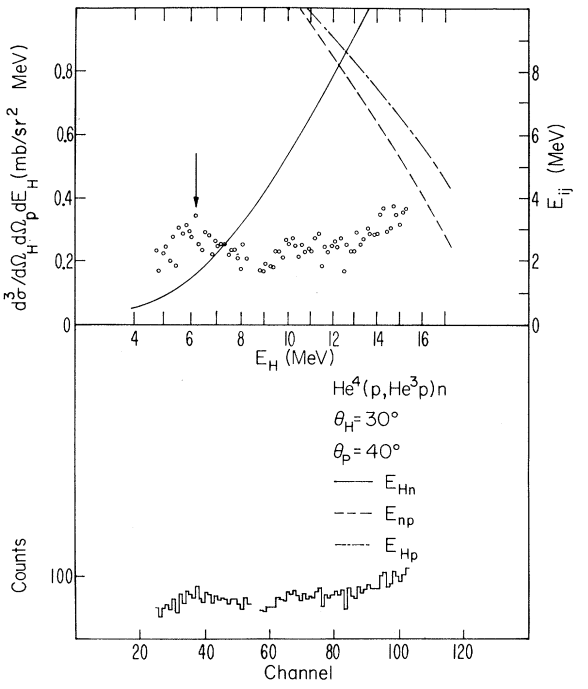

FIG. 21. He^3 spectrum: See the caption for Fig. 19.

ing to the 0^+ level and p-wave resonance in He^4, but not for any other levels. These measurements are in substantial agreement with ours as to the general character of the 0^+ and p-wave levels.

Inelastic proton spectra from $He^4(p,p')$ reactions measured at $E_p = 40$ MeV[19] show the 0^+ level to have an apparent width of 0.34 ± 0.04 MeV, considerably larger than the width we measure. The cause of the discrepancy in the measured width with these two different methods of studying the same reactions is not clear at this time.

SUMMARY AND CONCLUSIONS

Nucleon-Nucleon FSI

The energy spectra in the region of the second maximum of the trion angular distribution is in good agreement with the predictions of simple sequential theory. A Chew-Low type of extrapolation yields a value for the *np* singlet scattering length that is slightly lower than the value extracted from *np* free scattering. Because these experiments show no marked contradictions between the data and simple sequential theory, it seems worthwhile to undertake a study of the analogous reactions induced by fast neutrons on He^4, with a view towards simultaneously examining the *np* and *nn* FSI.

He^4 Levels

These reactions offer a convenient way to observe the resonance structure of He^4, since a large range of excitation energies is allowed in a measurement at a single bombarding energy and angle. The states of lowest excitation (0^+, 0^-, and/or 2^-) show up quite clearly. Of course the difficulties inherent in any analysis of three-body final states are present here, too, in that the reliable methods (e.g., phase-shift analysis) used to extract level parameters from two-body data are not available.

ACKNOWLEDGMENTS

Our sincere thanks go to J. M. Cameron for suggesting these experiments and for contributing generously to the early stages of their development. We are grateful to M. B. Epstein for extensive contributions to the data collection and for rewarding discussions. W. H. Dunlop was invaluable in his assistance with various computer programs and for help with the data acquisition. Discussions with W. E. Meyerhof and T. A. Tombrello were also valuable, and we gratefully acknowledge their contributions to the interpretation of the data.

These experiments would not have been possible without the skillful operation of the UCLA cyclotron by the technical staff, and the fabrication of mechanical equipment by the artists of the cyclotron machine shop.

---

*Present address: Texas A&M Cyclotron Institute, College Station, Texas.

†Present address: Institute Ruder Bošković, Zagreb, Yugoslavia.

‡Work supported in part by the U. S. Atomic Energy Commission, Contract No. AT-(11-1)-GEN 10 P.A. 18.

[1]E. L. Petersen, R. Bondelid, P. Tomaš, G. Paić, J. R. Richardson, and J. W. Verba, Phys. Rev. 188, 1497 (1969); E. Bar-Avraham, C. C. Chang, H. H. Forster, C. C. Kim, J. R. Richardson, P. Thomaš, and J. W. Verba, University of California, Los Angeles, Annual Report No. AR-3, 1968 (unpublished); E. Bar-Avraham, R. F. Carlson, C. C. Chang, H. H. Forster, C. C. Kim, J. R. Richardson, I. Slaus, P. Tomaš, W. T. H. van Oers, and J. W. Verba, J. Phys. Soc. Japan 24, 80 (1967).

[2]J. G. Rogers, J. M. Cameron, M. B. Epstein, G. Paić, P. Tomaš, J. R. Richardson, J. W. Verba, and P. Doherty, Nucl. Phys. A136, 433 (1969).

[3]S. N. Bunker, J. M. Cameron, M. B. Epstein, G. Paić, J. R. Richardson, J. G. Rogers, P. Tomaš, and J. W. Verba, Nucl. Phys. A133, 537 (1969).

[4]J. M. Cameron, J. R. Richardson, W. T. H. van Oers, and J. W. Verba, Phys. Rev. 167, 908 (1968).

[5]E. Bar-Avraham and L. C. Lee, Nucl. Instr. Methods 64, 141 (1968).

[6]J. G. Rogers, to be published.

[7]K. M. Watson, Phys. Rev. 88, 1163 (1952); A. B. Migdal, Zh. Eksperim. i Teor. Fiz. 28, 3 (1955) [transl.: Soviet Phys.–JETP 1, 2 (1955)]; T. A. Tombrello and A. D. Bacher, Phys. Letters 17, 37 (1965).

[8]M. A. Preston, *Physics of the Nucleus* (Addison-Wesley Publishing Company, Inc., Reading, Massachusetts, 1962), pp. 23–25.

[9]H. Brückman, W. Kluge, H. Matthäy, L. Schänzler, and K. Wick, Phys. Letters 30B, 460 (1969); C. C. Chang, E. Bar-Avraham, H. H. Forster, C. C. Kim, J. R. Richardson, and J. W. Verba, Phys. Letters 28B, 175 (1968); E. W. Blackmore and J. B. Warren, Can. J. Phys. 46, 233 (1968).

[10]M. Bernas, J. K. Lee, D. Bachelier, I. Brissaud, C. Detraz, P. Radvanyi, and M. Roy, Phys. Letters 25B, 260 (1967).

[11]W. E. Meyerhof and T. A. Tombrello, Nucl. Phys. A109, 1 (1968).

[12]H. Brückman, W. Kluge, and L. Schänzler, Phys. Letters 24B, 649 (1967).

[13]R. Hagedorn, *Relativistic Kinematics* (W. A. Benjamin, Inc., New York, 1964), Chap. 7.

[14]H. P. Noyes, *Few Body Problems, Light Nuclei, and Nuclear Interactions* (Gordon and Breach Publishers, Inc., New York, 1968).

[15]J. G. Rogers, University of California, Los Angeles,

Technical Report No. P-84, 1969 (unpublished).
[16]J. C. Legg, W. D. Simpson, and S. T. Emerson, Nucl. Phys. A119, 209 (1968).
[17]P. D. Parker, P. F. Donovan, J. V. Kane, and J. F. Mollenauer, Phys. Rev. Letters 14, 15 (1965); P. F. Donovan, Rev. Mod. Phys. 37, 501 (1965).
[18]R. W. Zurmühle, Nucl. Phys. 72, 225 (1965); R. W. Newsome, Bull. Am. Phys. Soc. 12, 17 (1967).
[19]L. E. Williams, Phys. Rev. 144, 815 (1966).

PHYSICAL REVIEW C VOLUME 2, NUMBER 3 SEPTEMBER 1970

R-Matrix Expansion for the Ground-State Energy of a Many-Fermion System*

George A. Baker, Jr., Margaret F. Hind, and Joseph Kahane
Applied Mathematics Department, Brookhaven National Laboratory, Upton, New York 11973
(Received 6 April 1970)

The *R*-matrix expansion for the ground-state energy of a many-fermion system is carried through fourth order. We evaluate this expansion for a potential modeled after the nucleon-nucleon one. The calculation is described in detail. We find that the "hole-line" approximation seems to underestimate the attraction so that a hard-core force may well be consistent with the experimental binding energy of large nuclei.

1. INTRODUCTION AND SUMMARY

A method, the *R*-matrix expansion, has recently been proposed[1,2] for the calculation of the ground-state energy of a many-fermion system interacting through forces which have a short-range strong repulsion, an intermediate-range attraction, and which vanish rapidly at long distances. It is the purpose of this paper to carry through such a calculation for a simple model potential, patterned on the nucleon-nucleon potential. The results of this calculation are compared with those of the two-"hole-line" approximation, and it appears that the "hole-line" approach substantially underestimates the binding energy in this case. Consequently it seems likely that hard-core potentials are compatible with the "observed values" for the binding energy for infinite nuclear matter.

In the second section of this paper we describe how to obtain the *R* matrix from the potential, both in the absence and presence of an excitation of the Fermi sea. The *R* matrix is basically the same as Brueckner's[3] *K* matrix except that it has been regularized[2] in the neighborhood of the Fermi surface to eliminate the appearance of certain singularities which occur in the Brueckner formulation.

Since the *R*-matrix expansion procedure involves multidimensional integrals of products of the *R* matrix elements, just as the potential perturbation expansion involved multidimensional integrals of products of the potential matrix elements, we have found it desirable to have an accurate numerical representation of the *R* matrix. We describe our representation in the third section. As a guide to the proper forms to employ, we compute the dilute limiting case, introduce adjustable parameters, and fit them to our values of the matrix elements computed by methods of the second section.

In Ref. 1, the spin and isospin sums were left in matrix form under the integrand of the multidimensional integrals. We have, however, found group-theoretic methods to reduce by mechanical procedures all of these sums (at least through the fourth order in the *R* expansion) *ab initio*. These procedures are described in the fourth section of this paper.

In the fifth section of our paper we detail how to write out the *R*-matrix perturbation series and give all the data necessary to construct the multidimensional integrals whose evaluation is required. In the final section we describe our evaluation of these integrals by Monte Carlo methods and tabulate the numerical results. Comparisons are made with the results of other methods.

2. EVALUATION OF THE *R* MATRIX

In order to evaluate the terms of the *R*-matrix expansion of the ground-state energy of a many-fermion system which was recently proposed,[1,2] we need first to evaluate the *R* matrix itself in terms of an interaction potential. We have selected the following potential for consideration in this paper. First, for states of even relative angular momentum,

$$\begin{aligned} &V_T(r) = V_1\,, \quad V_S(r) = V_2\,, \quad 0 < r < c\,, \\ &V_T(r) = V_3\,, \quad V_S(r) = V_4\,, \quad c < r < d\,, \\ &V_T(r) = V_S(r) = 0\,, \quad\quad\quad d < r\,, \end{aligned} \tag{2.1}$$